Appl Phys A (2010) 98: 557–563
DOI 10.1007/s00339-009-5507-5

Applied Physics A
Materials Science & Processing

Investigation of low-temperature electrical conduction mechanisms in highly resistive GaN bulk layers extracted with Simple Parallel Conduction Extraction Method

A. Yildiz · S.B. Lisesivdin · M. Kasap · S. Ozcelik · E. Ozbay · N. Balkan

Received: 21 August 2009 / Accepted: 25 November 2009 / Published online: 3 December 2009
© Springer-Verlag 2009

Abstract The electrical conduction mechanisms in various highly resistive GaN layers of $Al_xGa_{1-x}N/AlN/GaN/AlN$ heterostructures are investigated in a temperature range between $T = 40$ K and 185 K. Temperature-dependent conductivities of the bulk GaN layers are extracted from Hall measurements with implementing simple parallel conduction extraction method (SPCEM). It is observed that the resistivity (ρ) increases with decreasing carrier density in the insulating side of the metal–insulator transition for highly resistive GaN layers. Then the conduction mechanism of highly resistive GaN layers changes from an activated conduction to variable range hopping conduction (VRH). In the studied temperature range, $\ln(\rho)$ is proportional to $T^{-1/4}$ for the insulating sample and proportional to $T^{-1/2}$ for the more highly insulating sample, indicating that the transport mechanism is due to VRH.

A. Yildiz
Department of Physics, Faculty of Science and Arts, Ahi Evran University, Aşıkpaşa Kampüsü, 40040 Kirsehir, Turkey

A. Yildiz
Department of Engineering Physics, Faculty of Engineering, Ankara University, 06100 Besevler, Ankara, Turkey

S.B. Lisesivdin (✉) · E. Ozbay
Nanotechnology Research Center, Bilkent University, 06800 Bilkent, Ankara, Turkey
e-mail: sblisesivdin@gmail.com
Fax: +90-312-2901015

M. Kasap · S. Ozcelik
Department of Physics, Faculty of Science and Arts, Gazi University, 06500 Teknikokullar, Ankara, Turkey

E. Ozbay
Department of Physics, Bilkent University, 06800 Bilkent, Ankara, Turkey

E. Ozbay
Department of Electrical and Electronics Engineering, Bilkent University, 06800 Bilkent, Ankara, Turkey

N. Balkan
School of Computer Science and Electronic Engineering, University of Essex, CO4 3SQ Colchester, UK

1 Introduction

GaN and its related alloys have received considerable attention due to their important applications in both electronic and optoelectronic devices [1, 2]. In materials like GaN and its related alloys having a high energy gap [3, 4], impurity band conduction may be significant even at high temperatures [5–7]. Electrical conductivity processes in such materials having wide energy gaps are mainly due to carrier hopping within the impurity centers at low temperatures [5, 8, 9].

There have been a number of different efforts to determine electrical properties of GaN and its related alloys [5, 7, 10, 11]. Among the most important assessment methods is the Hall effect measurement which is most convenient for the investigation of the electrical properties of GaN and related alloys. It was reported that the conduction mechanism of highly degenerate Ga-rich $In_xGa_{1-x}N$ layers can be well explained by a model that takes into account electron–electron interactions and weak localization effects [6, 7]. Fehrer et al. [10] showed that the electrical properties of highly resistive GaN layers are mainly determined by potential barriers which are proposed to be localized at grain boundaries. Bhattacharyya and Pal [11] reported that VRH conduction dominate the carrier transport mechanism in GaN thin films at temperature range of 200–300 K.

Highly resistive GaN layers are mostly used to decrease the influence of the buffer on the main conducting layer [12]. However, there is always an expected parallel conducting channel in the buffer. The temperature-dependent Hall data of highly resistive GaN layers with a resistivity higher than 10^3 Ω cm could not be measured even at 400 K [13]. The studies on the electrical transport properties of highly resistive GaN layers are still limited.

Since the carriers in different conducting channels do not all have the same drift velocity, single magnetic field Hall measurements can only give an approximate result about the carriers in a GaN-based HEMT structures as it is the case in this study. There may be an important parallel conducting channel even for the unintentionally doped structure [14, 15]. To extract the contributions of 2DEG conductivity and parallel conductivity in our structure, the simple parallel conduction extraction method (SPCEM) is used [16].

The analysis of magnetic field dependent resistivity and Hall data have been discussed in several papers [17–19] for the parallel conduction problem with the methods like: two-carrier model [20], multi-carrier fitting procedure (MCF) [21], mobility-spectrum analysis (MSA) [22], MCF and MSA hybrid [23], and the quantitative mobility spectrum analysis (QMSA) package [24]. QMSA is well known to be superior to other existing methods. It has no limits for the carrier type and number of channels. However, in order to extract the effect of low mobility bulk carriers, very large magnetic fields ($\mu_{\min} B_{\max} \gg 1$) and stable thermal conditions required for long durations during the Hall measurements. SPCEM is recently proposed by Lisesivdin et al. [16] to extract the contributions of bulk and 2DEG carriers in a HEMT or MODFET structure. Therefore there are some assumptions in the method:

(1) There are two main contributions to conductivity: 2DEG carrier and a bulk carrier.
(2) At the low temperatures, bulk carriers are assumed to be frozen totally. Therefore, the measured Hall carrier density at the lowest temperature is accepted as the temperature-independent 2DEG carrier density [25].
(3) The change in temperature-dependent measured carrier density is caused by thermal activation of bulk carriers only.
(4) Densities of bulk carriers and the 2DEG are in the same order.

In the Lisesivdin et al.'s study [16], the following equations were found for the mobilities of 2DEG carrier (named as carrier 1) and bulk carrier (named as carrier 2) with the investigation of magnetic-field-dependent conductivity tensors and their derivatives:

$$\mu_1 \cong \mu_H^{\mathrm{Lo}} \sqrt{\frac{n_H^{\mathrm{Lo}}}{n_1^{\mathrm{Lo}}}}, \tag{1}$$

$$\mu_2 \cong \mu_H^{\mathrm{Hi}} \frac{n_H^{\mathrm{Hi}} - n_1^{\mathrm{Hi}}}{n_H^{\mathrm{Hi}}} = \mu_H^{\mathrm{Hi}} \frac{n_2^{\mathrm{Hi}}}{n_H^{\mathrm{Hi}}}. \tag{2}$$

Here, $\mu_H^{\mathrm{Lo}}, n_H^{\mathrm{Lo}}, \mu_H^{\mathrm{Hi}}, n_H^{\mathrm{Hi}}$ are Hall mobilities and Hall carrier densities at low magnetic fields and at high magnetic fields, respectively. Temperature-independent 2DEG carrier densities are calculated with $n_1^{\mathrm{Lo}} = n_H^{\mathrm{Lo}}$ and $n_1^{\mathrm{Hi}} = n_H^{\mathrm{Hi}}$ at the lowest temperature available. For the bulk carrier density contribution at each temperature step, $n_2^{\mathrm{Lo}} = n_H^{\mathrm{Lo}} - n_1^{\mathrm{Lo}}$ and $n_2^{\mathrm{Hi}} = n_H^{\mathrm{Hi}} - n_1^{\mathrm{Hi}}$ are used.

In this work, we investigated the Hall results in $\mathrm{Al}_x\mathrm{Ga}_{1-x}$N/AlN/GaN/AlN heterostructures with SPCEM for the first time in order to evaluate the contribution of the low-mobility carriers in GaN layers to total conductivity. The calculated electrical resistivity data from these undoped highly resistive GaN layers are investigated in a temperature range of 40–185 K.

2 Experimental

The samples in this study were all grown on c-plane (0001) sapphire (Al_2O_3) substrate with a low-pressure MOCVD reactor. Hydrogen was used as the carrier gas; trimethylgallium (TMGa), trimethylaluminum (TMAl), and ammonia were used as Ga, Al, and N precursors, respectively. Three samples were chosen for the present study. Samples A and B have the same growth conditions except the GaN buffer growth time which concludes different GaN buffer thicknesses. Sample C has different growth conditions with respect to other samples to present the general applicability of the analysis for these types of structures. All layers are nominally undoped. Sample layer thicknesses are listed in Table 1. Layer thicknesses and Al mole fraction values are checked using XRD and ellipsometry measurements.

For the Hall measurements by using the van der Pauw method, square-shaped (5 × 5 mm^2) samples were prepared with four evaporated triangular Ti/Al/Ni/Au (200 Å/2000 Å/300 Å/700 Å) contacts in the corners. Contacts are annealed with rapid thermal annealing (RTA) system. Ohmic behavior of the contacts was confirmed by the current voltage

Table 1 Layer thicknesses of the investigated samples

	Sample A	Sample B	Sample C
GaN cap (nm)	10.6	10.6	3.0
$\mathrm{Al}_x\mathrm{Ga}_{1-x}$N Barrier (nm)	18.8	18.8	27.0
AlN interlayer (nm)	∼1.0	∼1.0	∼1.5
GaN buffer (µm)	1.97	2.77	1.90
AlN buffer (µm)	0.72	0.72	0.60
AlN nucleation (nm)	11.2	11.2	15.0
Al mole fraction (x)	0.25	0.25	0.22

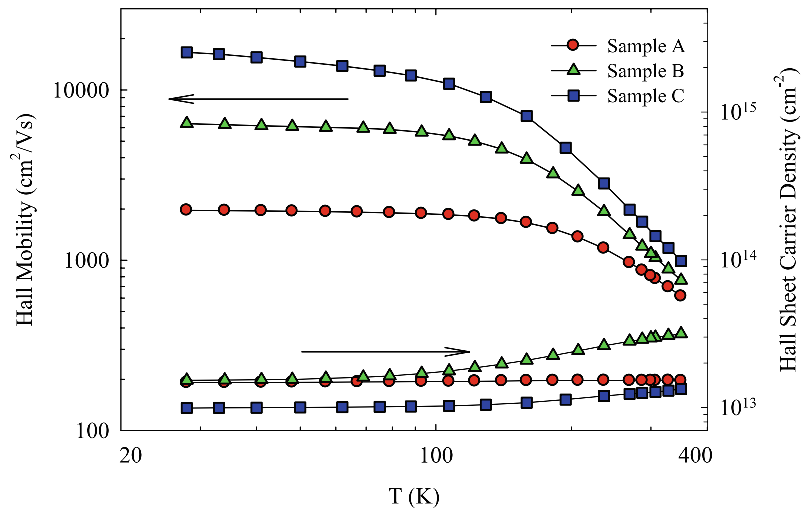

Fig. 1 Temperature-dependent Hall mobilities and Hall sheet carrier densities of the investigated samples

(I/V) characteristics. The measurements were taken in a temperature range of 28–350 K using a Lakeshore Hall effect measurement system (HMS). At temperature steps, the Hall coefficient (with max. 5% error) and resistivity (with max. 0.2% error in the studied range) were measured for both current directions, magnetic field polarizations, and all possible contact configurations. The low (0.05 T) and high (1.4 T) magnetic-field-dependent data has been used to calculate 2DEG and Bulk contributions in the investigated samples [16].

3 Result and discussion

Figure 1 shows the temperature dependence of Hall mobilities and Hall sheet carrier densities of the investigated $Al_xGa_{1-x}N/AlN/GaN/AlN$ heterostructures at $B = 1.4$ T in a temperature range between $T = 28$ K and 350 K. At room temperature, Hall mobilities are 809, 1095, and 1471 $cm^2/V\,s$, Hall sheet carrier densities are 1.52×10^{13}, 2.96×10^{13}, and 1.28×10^{13} cm^{-2} for the samples A, B, and C, respectively. At 28 K, Hall mobilities are as high as 1963, 6335, and 16621 $cm^2/V\,s$ for the samples A, B, and C, respectively. These mobility and carrier density behaviors are typical for samples that have dominant 2DEG conduction [26].

To calculate 2DEG and bulk contributions, SPCEM analysis is carried out with using the low-magnetic-field (0.05 T) and high-magnetic-field (1.4 T) Hall data as the input. SPCEM results are shown in Fig. 2. Sample A has the lowest mobilities and carrier densities for both 2DEG and bulk contributions. Sample B has the highest mobility and carrier density for its bulk contribution. Sample C has the highest mobility for 2DEG contribution. Carrier mobilities of all the layers are influenced by the polar optical phonon scattering at high temperatures [27] as expected

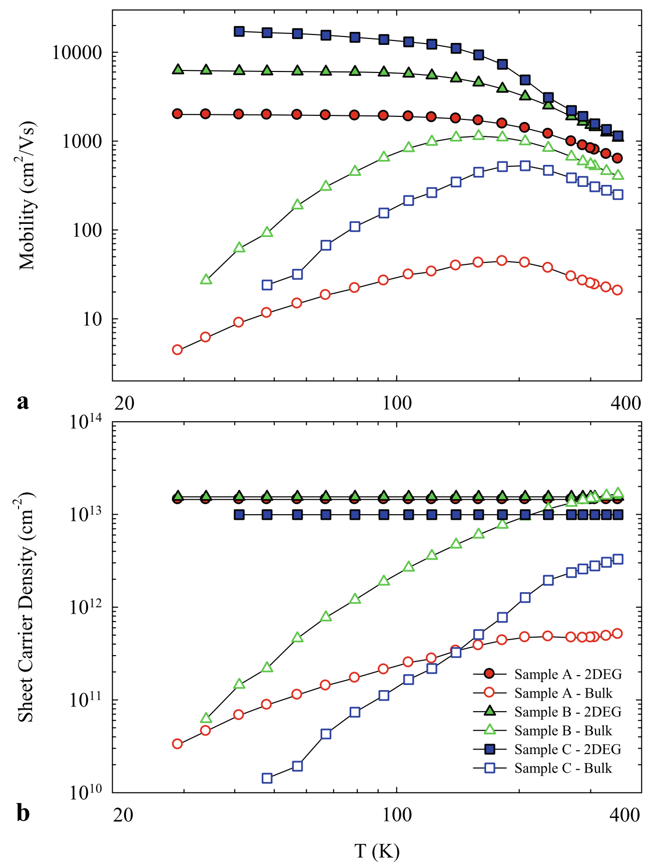

Fig. 2 Calculated (**a**) mobilities and (**b**) sheet carrier densities of the bulk (*empty symbols*) and 2DEG (*filled symbols*) carriers after implementing SPCEM

from a highly polar material. The bulk mobilities decrease further with decreasing temperature as expected because of local ionized impurity scattering [28]. For all three samples, SPCEM works well, and the results compare well with those for a GaN-based system [26, 28].

Table 2 Properties of GaN layers; room temperature values of carrier density (n), mobility (μ), and resistivity (ρ)

Sample	n (cm^{-3})	μ ($cm^2/V\,s$)	ρ ($\Omega\,cm$)
A	2.38×10^{15}	25	5.34×10^5
C	2.26×10^{16}	467	3.11×10^3
B	5.35×10^{16}	548	7.71×10^2

Electrical components of highly resistive bulk GaN layers; resistivity (ρ), mobility (μ), and carrier density (n) are shown at room temperature in Table 2. Knowing μ and n values previously, the resistivities for the bulk GaN layers are determined using the relation $\rho^{-1} = en\mu$, where e is the electron charge. The layers indicate n-type behavior, which can be due to the presence of nitrogen vacancy. The highest mobility value (548 $cm^2/V\,s$) belongs to sample B with the lowest resistivity value (7.71×10^2 $\Omega\,cm$). As the carrier densities of the GaN layers decreases, the mobility decreases hence the resistivity increases. Then, the samples go to insulating side of the metal–insulator transition. For an effective mass of $m^* = 0.22m_0$ [29, 30] and static dielectric constant of $\varepsilon = 10.4$ [29, 30], Bohr radius can be calculated as $a_B = 2.51$ nm for electrons in a donor band of GaN. The critical density for the metal–insulator transition is then [31] $n_c = (0.25/a_B)^3 = 9.9 \times 10^{17}$ cm^{-3}. This suggests that for $n > 9.9 \times 10^{17}$, the conduction is "metallic like" in GaN, where n is the carrier density. Below this value the conduction takes place by phonon assisted hopping. As seen from Table 2, all GaN layers with $n < n_c$ fall in the insulating side of the metal–insulator transition. On the insulator side of the metal–insulator transition, thermally activated tunneling between impurity sites is the dominant conduction mechanism [32, 33]. The low-temperature resistivity in a three dimensional system is [32, 33]

$$\rho(T) = \rho_0 \exp\left(\frac{T_0}{T}\right)^s, \tag{3}$$

where ρ_0 is the preexponential factor, and T_0 is a characteristic temperature. The value of $s = 1$ corresponds to the nearest-neighbor hopping (NNH) mechanism or simply activated hopping. In the NNH mechanism, the resistivity is proportional to $\exp(\varepsilon_3/kT)$, and electron with ε_3 activation energy hops to the nearest neighboring empty site. The activation energy ε_3 is much smaller than the activation energy required for thermally activated band to band conduction. However, when VRH mechanism dominates in the conduction, the condition $0 < s < 1$ is fulfilled. If the density of states around the Fermi level assumed to be constant, s becomes $s = 1/4$ (Mott VRH). On the other hand, if there is a gap at the Fermi level, the VRH conduction model is expressed with $s = 1/2$ in (3) (ES VRH) [32, 33].

Since hopping conduction model is applicable at low temperatures [32, 33], we consider only the resistivity data

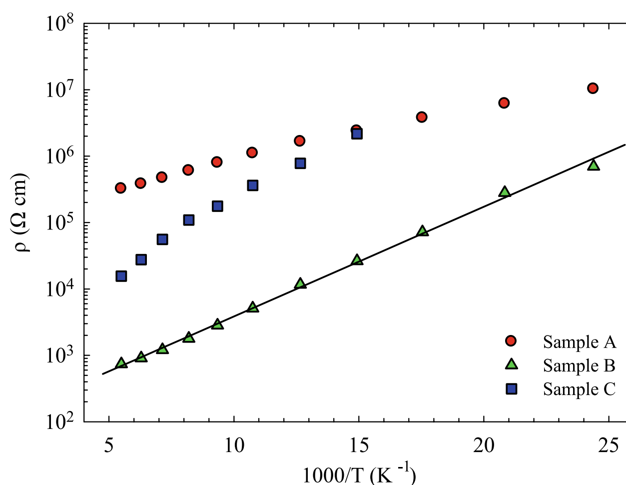

Fig. 3 Variation of the resistivity with inverse temperature for GaN layers. The *line* is the least square linear fit to the data of sample B

of GaN layers at temperatures below 185 K, where the impurity band conduction may start to dominate. In a temperature range of 28–185 K, especially at temperatures between 40 and 185 K, very good linearity on the temperature-dependent resistivity plots (Figs. 3–5) is observed. Figure 3 shows $\ln\rho$ versus $1/T$ plots for GaN layers in a temperature range of 40–185 K. It is clear that ρ increases as T decreases for all samples. However, linearity with $1/T$ is observed for only sample B in Fig. 3. This may suggest that the conductivity over this range of temperature is characterized by a constant activation energy of about $\varepsilon_3 = 33$ meV. For GaN, donor levels in the 0.25–0.45 eV range, evaluated from the thermally activated conductivity, and it is attributed to nitrogen vacancies [34]. Hence, the possibility of NNH conduction or simply activated conduction that arises from donor levels is to be confirmed for sample B with the activation energy of 33 meV. On the other hand, a reasonable straight line in Fig. 3 cannot be drawn through the points for samples A and C. The plots suggest that there is mixed conductivity, i.e., there are different contributions to conduction channels in these samples. The resistivity data of these samples can be fitted with the VRH models proposed by Mott [32] and Efros–Shklovskii [33]. In order to confirm that VRH was occurring, it is necessary to test either for the Mott VRH $T^{-1/4}$ law or for the ES VRH $T^{-1/2}$ law. The best correlation coefficient for sample C is obtained in Fig. 4, which shows the variation of $\ln(\rho)$ with $T^{-1/4}$ (Mott VRH) between 40–185 K. However, the plot of $\ln(\rho)$ vs. $T^{-1/2}$ (Fig. 5) is found to be linear for sample A. When the measured data is plotted as $\ln(\rho)$ versus $T^{-1/2}$ as indicated by the ES VRH, a well-defined line is obtained for sample A.

From the slopes of plots of Figs. 4 and 5, the values of Mott's and ES's characteristic temperatures are obtained as $T_{0,\mathrm{Mott}} = 1.54 \times 10^7$ K and $T_{0,\mathrm{ES}} = 1.81 \times 10^3$ K for sam-

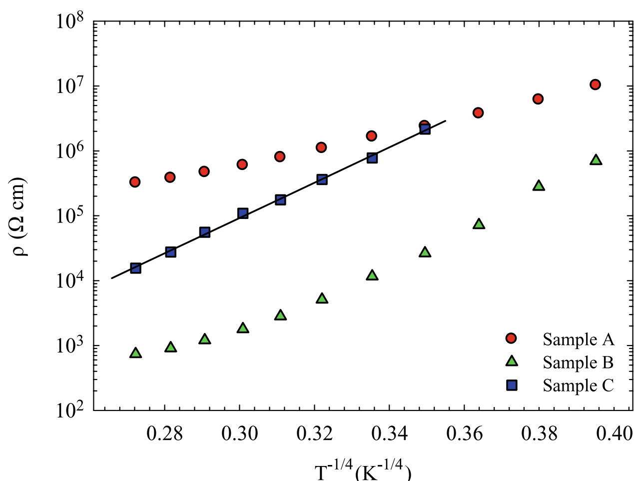

Fig. 4 Resistivity vs. $T^{-1/4}$ dependence for GaN layers. The *line* is the least square linear fit to the data of sample C

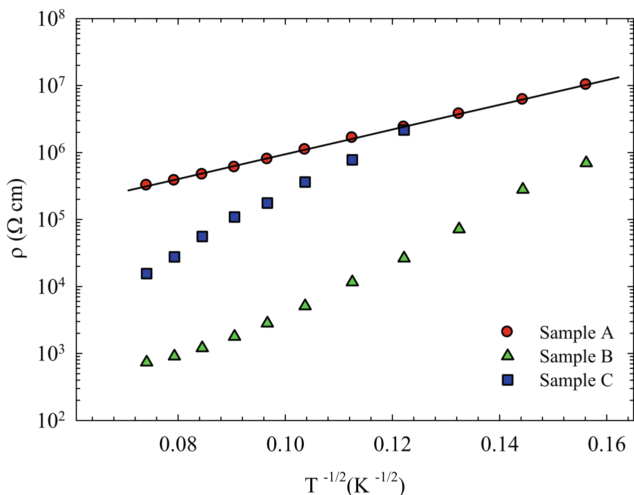

Fig. 5 Resistivity vs. $T^{-1/2}$ dependence for GaN layers. The *line* is the least square linear fit to the data of sample A

ples C and A, respectively. However, this simple graphical analysis is not an appropriate way to decide which hopping conduction mechanism dominates the conduction. In order to obtain the value of the exponent s with more accurately in the GaN layers, we analyze the ρ versus T data using the approach of Zabrodskii and Zinoveva [35]:

$$W(T) = -d\big[\ln \rho(T)\big]/d\big[\ln(T)\big]. \tag{4}$$

$W(T)$ can be used to determine metallic and insulating behavior of the conductivity. When the slope of $\ln(W(T))$ v.s. $\ln(T)$ is negative, that is, W increases as T decreases, the system is in the insulating side of MIT. The positive slope of the W plot indicates that the system can be in the metallic regime [35]. Figure 6 shows the plots of $\ln[W(T)]$ vs. $\ln(T)$ for the investigated samples. The slope of $W(T)$ of all samples is negative, implying that the samples are in

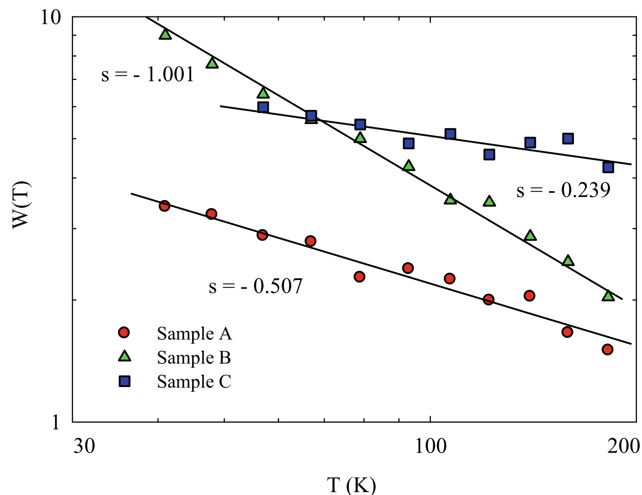

Fig. 6 Plot of $W(T) = -d[\ln \rho(T)]/d[\ln(T)]$ versus $\ln(T)$ for various GaN layers

the insulating regime. The values of s can be determined from the linear slope of Fig. 6. A linear fit for sample B yields a slope of -1.001, indicative of thermally activated conduction (NNH) mechanism. It is clear that exponent s (a slope of -0.239) is close to $1/4$ for sample C, which corresponds to Mott VRH. Decreasing carrier density in GaN layers leads to an observation to ES VRH, then a value of -0.507 is obtained for sample A.

A good fit of the measured data is essential, but not sufficient, criterion for applicability of the hopping theory. The hopping parameters should satisfy both NNH and VRH requirements. NNH activation energy ε_3 is given by [36]

$$\varepsilon_3 = \frac{e^2 N_D^{1/3}}{4\pi\varepsilon}, \tag{5}$$

where N_D is donor concentration, and ε is the static dielectric constant. From (5), the value of $N_D = 1.3 \times 10^{19}\ \text{cm}^{-3}$ is obtained for sample B. This value is seemed to be very high for this sample compared with room temperature carrier concentration $\sim 5.35 \times 10^{16}$. By a slope analysis of the electron concentration or resistivity versus reciprocal temperature data for GaN layers, the activation energy for donor ionization has been determined by several researches [36–39] using variable temperature Hall effect measurements. An activation energy ranging from 4 to 37 meV has been extracted for GaN [37–40]. The value of activation energy is $\varepsilon_3 = 33$ meV for GaN; this donor level may be due to act as a shallow donor and may contribute to the n-type background conductivity in unintentionally doped GaN [40]. This activation energy is mostly associated with Si, which is an expected residual donor impurity in the lattice [37–40].

On the other hand, the characteristic temperatures, $T_{0,\mathrm{Mott}}$ and $T_{0,\mathrm{ES}}$, obtained from the slopes of plots of Figs. 4 and 5 are theoretically expressed in the VRH regime as [32, 33]

$$T_{0,\mathrm{Mott}} = \frac{18\alpha^3}{k_B N(E_F)} \tag{6}$$

and

$$T_{0,\mathrm{ES}} = \frac{2.8e^2\alpha}{k_B\varepsilon}, \tag{7}$$

where α^{-1} is the localization length, $N(E_F)$ is the density of states at the Fermi level, e is the electron charge, and k_B is Boltzmann's constant. The value of α^{-1} can be assumed to be in the same order as the Bohr radius for GaN. Therefore, using the value of $T_{0,\mathrm{Mott}} = 1.54 \times 10^7$ K, we can easily estimate the quantity of $N(E_F)$ as 8.57×10^{17} $\mathrm{cm}^{-3}\,\mathrm{eV}^{-1}$ for sample C. This value is close to the previously reported value for GaN [5]. Also, knowing value of $T_{0,\mathrm{ES}}(1.81 \times 10^3$ K) in (7), value of the static dielectric constant, ε can be determined as 10.3 for sample A. This is in perfectly agreement with the generally accepted value ($\varepsilon = 10.4$ [29, 30]). These observations confirm that Mott and ES VRH mechanisms dominate on the electrical conduction in samples C and A, respectively. Therefore, we can also evaluate the other hopping parameters for these samples. For Mott VRH, the temperature-dependent hopping distance (R_{hop}) and average hopping energy (Δ_{hop}) are calculated from (8) and (9), respectively [32]:

$$R_{\mathrm{hop,Mott}} = 0.375(T_{0,\mathrm{Mott}}/T)^{1/4}\alpha^{-1}, \tag{8}$$

$$\Delta_{\mathrm{hop,Mott}} = 0.25k_B T(T_{0,\mathrm{Mott}}/T)^{1/4}. \tag{9}$$

Similarly, the temperature-dependent hopping distance (R_{hop}) and average hopping energy (Δ_{hop}) of the ES VRH conduction are given as follows [33]:

$$R_{\mathrm{hop,ES}} = 0.25(T_{0,\mathrm{ES}}/T)^{1/2}\alpha^{-1}, \tag{10}$$

$$\Delta_{\mathrm{hop,ES}} = 0.5k_B T(T_{0,\mathrm{ES}}/T)^{1/2}. \tag{11}$$

Using the values of $T_{0,\mathrm{Mott}}$, $T_{0,\mathrm{ES}}$, and α^{-1}, parameters are found as $R_{\mathrm{hop,Mott}} = 19.9$ nm, $\Delta_{\mathrm{hop,Mott}} = 35.1$ meV and $R_{\mathrm{hop,ES}} = 3.04$ nm, $\Delta_{\mathrm{hop,ES}} = 16.1$ meV at 77 K for samples C and A, respectively. Both the Mott VRH and ES VRH are valid if $R_{\mathrm{hop}} > \alpha^{-1}$ and $\Delta_{\mathrm{hop}} > k_B T$. Since $\alpha^{-1} = 2.51$ nm and $k_B T = 6.64$ meV ($T = 77$ K), both two conditions are well fulfilled at both Mott and ES regime for GaN layers.

In order to explain different transport behavior in the present samples, we considered the grain boundary model [41, 42]. Salzman et al. [43, 44] showed that the grain boundary model can be applicable to GaN epitaxial films like our case. As can be seen from Table 1, sample A and B have different GaN buffer thicknesses. The thickness of the films has a drastic effect on the resistivity, changing it by almost two orders of magnitude. When the grain boundary model [41, 42] is considered, we may explain the observed different transport behavior in our samples as follows: As the thickness decreases, the crystallite size decreases, and this leads to an increment in the trapping states at grain boundary. Trapping states are capable of trapping free carriers, and, as a consequence, more free carriers become immobilized as trapping states increases. On the other words, the larger crystallite size results in a lower density of grain boundaries, which behave as traps for free carriers and barriers for carrier transport in the film. Hence, an increase in the crystallite size can cause a decrease in grain boundary scattering, which leads to a decrease in the resistivity. Then, electrical properties are explained with different conduction models for our samples. Since the sample C has different growth conditions with respect to other samples, we do not compare sample C with other samples. Then it can be expected that sample C does not follow this trend.

4 Conclusions

Temperature-dependent Hall measurements of $\mathrm{Al}_x\mathrm{Ga}_{1-x}\mathrm{N}$/AlN/GaN/AlN are reported in a temperature range of 28–350 K. The contributions of bulk and 2DEG carriers are distinguished with SPCEM technique, and the results are shown to be in good agreement with those published in the literature. The electrical conduction mechanism in various highly resistive bulk GaN layers is investigated in a temperature range between $T = 40$ K and 185 K using bulk mobilities and carrier densities as extracted with the SPCEM technique. It is found that the conduction mechanism of highly resistive GaN layers changes from an activated to VRH conduction with decreasing carrier density. The resistivity is found to obey Mott VRH and ES VRH for insulating and highly insulating samples, respectively. Hopping parameters, such as the characteristic temperature (T_0), hopping distance (R_{hop}), average hopping energy (Δ_{hop}), dielectric constant (ε), and density of states ($N(E_F)$), are all determined from our measurements where we show that their values quite well agree with the assumptions of the Mott VRH and ES VRH mechanisms.

Acknowledgements This work is supported by the State of Planning Organization of Turkey under Grant No. 2001K120590, the European Union under the projects EU-PHOME, and EU-ECONAM, and TUBITAK under Project Nos. 106E198, 107A004, and 107A012. One of the authors (Ekmel Ozbay) acknowledges partial support from the Turkish Academy of Sciences.

References

1. S. Nakamura, S. Senoh, N. Iwasa, S. Nagahama, Jpn. J. Appl. Phys. **34**, L797 (1995)

2. Q. Chen, M.A. Khan, J.W. Yang, C.J. Sun, M.S. Shur, H. Park, J. Appl. Phys. **69**, 794 (1996)
3. H.P. Maruska, J.J. Tietjen, Appl. Phys. Lett. **15**, 327 (1969)
4. A. Yildiz, F. Dagdelen, S. Acar, S.B. Lisesivdin, M. Kasap, Y. Aydogdu, M. Bosi, Acta Phys. Pol. (a) **113**, 731 (2008)
5. R.K. Roy, S. Grupta, A.K. Pal, Thin Solid Films **483**, 287 (2005)
6. A. Yildiz, S.B. Lisesivdin, M. Kasap, D. Mardare, Opt. Adv. Mater.-Rapid Commun. **1**, 531 (2007)
7. A. Yildiz, S.B. Lisesivdin, M. Kasap, D. Mardare, J. Non-Cryst. Solids **354**, 4944 (2008)
8. A. Yildiz, S.B. Lisesivdin, S. Acar, M. Kasap, M. Bosi, Chin. Phys. Lett. **24**, 2930 (2007)
9. A. Yildiz, S.B. Lisesivdin, M. Kasap, D. Mardare, Physica B **404**, 1423 (2009)
10. M. Fehrer, S. Einfeldt, U. Birkle, T. Gollnik, D. Hommel, J. Cryst. Growth **189–190**, 763 (1998)
11. S.R. Bhattacharyya, A.K. Pal, Bull. Mater. Sci. **31**, 73 (1982)
12. H. Yu, M.K. Ozturk, S. Ozcelik, E. Ozbay, J. Cryst. Growth **293**, 273 (2006)
13. D.C. Look, D.C. Reynolds, W. Kim, O. Aktas, A. Botchkarev, A. Salvador, H. Morkoç, J. Appl. Phys. **80**, 2960 (1996)
14. E.F. Schubert, K. Ploog, H. Dämbkes, K. Heime, Appl. Phys. A **33**, 63 (1984)
15. I. Vurgaftman, J.R. Meyer, C.A. Hoffman, D. Redfern, J. Antoszewski, L. Farone, J.R. Lindemuth, J. Appl. Phys. **84**, 4966 (1998)
16. S.B. Lisesivdin, N. Balkan, E. Ozbay, Microelectron. J. **40**, 413 (2009)
17. J.S. Kim, D.G. Seiler, W.F. Tseng, J. Appl. Phys. **73**, 8324 (1993)
18. A. Wolkenberg, T. Przeslawski, J. Kaniewski, K. Reginski, J. Phys. Chem. Solids **64**, 7 (2003)
19. J. Antoszewski, L. Faraone, I. Vurgaftman, J.R. Meyer, C.A. Hoffman, J. Electron. Mater. **33**, 673 (2004)
20. M.J. Kane, N. Apsley, D.A. Anderson, L.L. Taylor, T. Kerr, J. Phys. C, Solid State Phys. **18**, 5629 (1985)
21. S.P. Tobin, G.N. Pultz, E.E. Krueger, M. Kestigian, K.K. Wong, P.W. Norton, J. Electron. Mater. **22**, 907 (1993)
22. W.A. Beck, J.R. Anderson, J. Appl. Phys. **62**, 541 (1987)
23. J.R. Meyer, C.A. Hoffman, F.J. Bartoli, D.J. Arnold, S. Sivananthan, J.P. Faurie, Semicond. Sci. Technol. **8**, 805 (1993)
24. J. Antoszewski, D.J. Seymour, L. Faraone, J.R. Meyer, C.A. Hoffman, J. Electron. Mater. **24**, 1255 (1995)
25. J.H. Davies, *The Physics of Low-Dimensional Semiconductors* (Cambridge University Press, Cambridge, 1998)
26. S.B. Lisesivdin, S. Demirezen, M.D. Caliskan, A. Yildiz, M. Kasap, S. Ozcelik, E. Ozbay, Semicond. Sci. Technol. **23**, 095008 (2008)
27. B.K. Ridley, J. Phys. C, Solid State Phys. **15**, 5899 (1982)
28. M. Shur, B. Gelmont, M. Asif Khan, J. Electron. Mater. **25**, 777 (1996)
29. H. Morkoç, *Nitride Semiconductors and Devices* (Springer, Heidelberg, 1999)
30. S.N. Mohammad, H. Morkoc, Prog. Quantum Electron. **20**, 361 (1996)
31. N.F. Mott, W.D. Twose, Adv. Phys. **10**, 107 (1961)
32. N.F. Mott, E.A. Davis, *Electronic Properties in Non-Crystalline Materials* (Clarendon, Oxford, 1971)
33. A.L. Efros, B.I. Shklovskii, *Electronic Properties of Doped Semiconductors* (Springer, Berlin, 1984)
34. T.L. Tansley, R.J. Egan, Physica B **185**, 190 (1993)
35. A.G. Zabrodskii, K.N. Zinoveva, Sov. Phys. JETP **59**, 425 (1984)
36. B.I. Shklovskii, Sov. Phys. Semicond. **6**, 1053 (1973)
37. M.A. Di Forte-Poisson, F. Huet, A. Romann, M. Tordjman, D. Lancefield, E. Pereira, J. Di Persio, B. Pecz, J. Cryst. Growth **195**, 314 (1998)
38. D.C. Look, D.C. Reynolds, J.W. Hemsky, J.R. Sizelove, R.L. Jones, R.J. Molnar, Phys. Rev. Lett. **79**, 2273 (1997)
39. P. Hacke, A. Maekawa, N. Koide, K. Hiramatsu, N. Sawaki, Jpn. J. Appl. Phys. **33**, 6443 (1994)
40. W. Götz, N.M. Johnson, C. Chen, H. Liu, C. Kuo, W. Imler, Appl. Phys. Lett. **6**, 3144 (1996)
41. J.Y.W. Seto, J. Appl. Phys. **46**, 5247 (1975)
42. J.W. Orton, M.J. Powel, Rep. Prog. Phys. **43**, 1263 (1980)
43. J. Salzman, C. Uzan-Saguy, R. Kalish, V. Richter, B. Meyler, Appl. Phys. Lett. **76**, 1431 (2000)
44. J. Salzman, C. Uzan-Saguy, B. Meyler, R. Kalish, Phys. Stat. Sol. (a) **176**, 683 (1999)